Current Biology, Volume *22*

Supplemental Information

Waking-like Brain Function in Embryos

Evan Balaban, Manuel Desco, and Juan-José Vaquero

Author Contributions

E.B. and J.-J.V. conceived the study; E.B., M.D., and J.-J.V. designed the experiments; E.B. and J.-J.V. carried out the experiments; E.B. analyzed the data; and E.B. and J.-J.V. wrote the paper.

Supplemental Inventory

Waking-like Brain Function in Embryos, *Current Biology* (2012)
http://dx.doi.org/10.1016/j.cub.2012.03.030

Supplemental Results

Additional Analyses of Embryo Brain Metabolic Patterns

Figure S2A shows the correlation between the maximum activity value in the telencephalon and the maximum activity value in cerebellum in individual birds ($r = 0.96$, $n = 201$, $p < 0.0001$). The correlation coefficients for embryos in the three sound stimulus conditions were identical to each other (Silence: $r = 0.96$, $n = 51$, $p < 0.001$; Filtered Noise: $r = 0.96$, $n = 51$, $p < 0.001$, Chicken Sound: $r = 0.96$, $n = 95$, $p < 0.001$).

Figure S2B shows the locations of metabolic activity within 15% of the higher-brain maximum, shared by at least 50% of the embryos within each brain pattern / developmental stage category, and transformed to a standard spatial template for each developmental stage. Activated areas included: [bilateral forebrain] hyperpallium / mesopallium; [cerebellum] a single region including the bilateral deep cerebellar nuclei; [ventral brainstem] rPRF (present in fActive embryos, but generally below 15% of the maximum value in the higher brain). The brain regions with the greatest activity were similar across all metabolic categories and developmental stages.

We conducted statistical analyses to see if there were any fluctuations in the proportion of different brain metabolic patterns with time of day (our experiments were conducted between 8:00-21:00); there were no significant differences in proportions among different time periods when the experimental times in this interval were divided into hourly periods, or into 3 periods – before 12:00, from 12:00-17:00, after 17:00 (all $p > 0.25$). Since the eggs were incubated in darkness, even if individual embryos had circadian variation in brain activation, the patterns would not necessarily be entrained among different embryos, and so would not show up as a population-level fluctuation.

Additional Analyses of Sound Stimulation Effects on Brain and Behavior

We divided the brain metabolic activation data by sound stimulus (chicken (C) and filtered noise (FN)) and developmental stage (Age II or Age IV) to examine the effects of stimulus duration. For the C-stimulation condition, there were no significant differences in the frequency of rActive embryos between 5-min and 15-min presentations (Age II: 43% for 5-min vs. 50% for 15-min; Age IV: both 89%), so we combined the data for these two presentation lengths within each developmental stage. There were no significant differences in the proportion of rActive brains produced by sound presentations of 2-min durations vs. the longer durations at either developmental stage for the filtered-noise or chicken stimuli (FN: Age II, $G = 0.03$, $p = 0.87$; Age IV, $G = 0.16$, $p = 0.69$; C: Age II, $G = 0.63$, $p = 0.43$; Age IV, $G = 2.83$, $p = 0.09$).

We did not find any reliable movement or heart-rate response differences temporally locked to stimulus presentation (that is, occurring within a 30-second period after the beginning of each sound stimulus, all $p > 0.20$). However, dynamic changes in the number and average duration of movement bouts did show differences when comparing the period 5 minutes before stimulation began (measured at an equivalent time in embryos exposed to silence) with the 5 minute period after stimulation began (Figure S3A). Here, rInactive embryos showed significantly different changes in both number and mean duration of movement bouts in sound-stimulated as compared to silent conditions (with sound-stimulated embryos showing relatively larger changes in both). This relationship held for the developmental periods prior to Age IV

(Mann-Whitney Tests, Sound (n = 42) vs. Silence (n = 11), movement number ratio: p = 0.004, movement duration ratio: p = 0.03), when rInactive embryos do not have quiescent period durations distributed like sleep, but not at Age IV (Sound (n = 15) vs. Silence (n = 10), movement number ratio: p = 0.78, movement duration ratio: p = 0.44). There were no stimulus-based differences in movement responses for pActive embryos, and fActive embryos showed significant differences in the ratio of both the number and mean duration of movements among all three stimulation conditions (with chicken-stimulated embryos having the largest changes in both).

Since rInactive embryos at Ages II/III and IV exhibited changes in behavior in response to sound stimulation, in the absence of major changes in the magnitude of glucose uptake in higher brain regions, we wondered if stimulation led to more subtle changes in the distribution of their brain glucose uptake patterns. Although there were no stimulus-related differences in the mean (first moment) or the variance (second moment) of the brain distributions (not shown), there were significant increases in skewness ("asymmetry", third moment, Kruskal-Wallis test, H = 14.54, df = 3, p = 0.0023) and kurtosis ("peakedness", fourth moment, Kruskal-Wallis test, H = 74.50, df = 3, p < 0.0001) [Figure S3B]. The biological interpretation of these changes is as follows. Brain metabolic activity values were distributed over a narrow range in rInactive embryos; sound stimulation caused a reliable shift of these values away from the center (around the "peak" of the distribution) and into the "tails" (producing the significant positive increase in kurtosis in the population of sound-stimulated rInactive embryos). There were reliably more relative increases in metabolic activation than decreases, so the "upper tails" of the brain distributions became longer than the "lower tails" (producing the significant positive increase in skewness). The means did not change significantly because the overall effects of these positive and negative shifts partially cancelled each other; the variance did not significantly increase because the changes in value were not extreme enough. Posthoc tests corrected for multiple comparisons ($p < 0.05$) showed that significant changes to sound stimulation occurred in these parameters for rInactive but not rActive brains (Figure S3B).

Significant differences also occurred in the spatial extent of activation in the cerebellar and telencephalic regions identified in Figure S2B. In the cerebellum, the volume of activation at 85% of the maximum value was significantly smaller in sound-stimulated rInactive embryos than in silent ones (Kruskal-Wallis test, H = 9.45, df = 2, p = 0.009; posthoc tests corrected for multiple comparisons, $p < 0.05$, Figure S3C, left), while the telencephalic volume of activation was smaller in filtered-noise-stimulated rInactive embryos than in the two other groups (Kruskal-Wallis test, H = 7.34, df = 2, p = 0.026; posthoc tests corrected for multiple comparisons, $p < 0.05$, Figure S3C, right).

The developmentally least-advanced (Age 1) rInactive embryos also showed behavioral and brain response differences to stimulation. Embryos exposed to the filtered-noise stimulus showed greater values of normalized movement duration change (the average movement duration during the 5 minutes after stimulation minus the average during the five minutes before stimulation, divided by the overall mean movement duration; mean$\pm$ sd: S (n = 5), -2.4 $\pm$ 5.5 %; FN (n = 10), 19.0 $\pm$ 5.4 %; C (n = 9), -5.1 $\pm$ 6.7 %; Kruskal-Wallis test: H = 6.36, df = 2, p = 0.042). Filtered-noise-stimulated embryos were also the only ones with change values significantly greater than zero (Wilcoxon tests corrected for 3 comparisons, $p > 0.95$ for S,C stimuli, p = .038 for FN). This behavioral variable also had significantly different correlations

with the telencephalic volume of activation for filtered-noise- and chicken-sound-stimulated Age 1 embryos (FN: r = -0.71, n = 10, p = 0.019; C: r = 0.52, n = 9, p = 0.16; S: r = -0.13, n = 5, p = 0.86; χ^2 for heterogeneity = 6.88, df = 2, p < 0.032; multiply-corrected FN-C comparison, p< 0.026, C-S and FN-S comparisons both p > 0.95). This demonstrated that the lack of rActive brain responses observed at Age I was not due to either a lack of transmission of external sensory information to the brain, or a lack of responsiveness of the brain to sensory stimulation.

Additional Analyses of Stimulus-Exclusive Induction of Correlated Activity between Brain Areas

Approximately 33 % (15-min-stimulated embryos excluded) - 40 % (15-min-stimulated embryos included) of all chicken-stimulated fActive embryos had elevated rPRF levels and MRF/rPRF ratios (respective p-values are 0.042 and 0.0009, df = 1, relative to 0 % for non-chicken-stimulated fActive embryos, Fisher's exact test). Excluding embryos stimulated for 15-minutes, chicken- and filtered-noise-stimulated fActive embryos also had significantly different, oppositely-signed correlations between rPRF glucose uptake and MRF/rPRF ratios (C: r = 0.79, n = 15; FN: r = -0.34, n = 7; difference, p = 0.008). The group of chicken-stimulated fActive embryos with elevated rPRF maxima and MRF/rPRF ratios also had significantly higher glucose uptake levels in the telencephalon and cerebellum (Kruskal-Wallis test, H = 14.05, df = 2, p = 0.009, 15-min birds included; H = 9.20, df = 2, p = 0.01, 15-min birds excluded, Figure S4A), and a larger increase in the number of movement bouts after stimulation than other fActive embryos (H = 6.81, df = 2, p = 0.03 Figure S4B); all chicken-stimulated fActive embryos also had greater post-stimulation changes in movement bout length than their counterparts (H = 8.43, df = 2, p = 0.015, Figure S4C).

Figure S5 shows the correlation between rPRF maxima and telencephalon / cerebellum maxima divided according to developmental stage. The probabilities were corrected for 12 comparisons [2 developmental stages (Ages II/III, and IV) x 2 brain patterns (rInactive, rActive) x 3 stimulus conditions (S [silent], FN [filtered noise], C [chicken])]; none of the S or FN correlations were significant. The correlation is significantly positive for rInactive and (marginally) for rActive embryos at Age II / III, and for rActive embryos only at Age IV. Therefore, chicken-stimulation resulted in a correlation between metabolic activity in the brainstem and higher brain at all developmental stages where stimulation affected the magnitude of higher-brain glucose metabolic responses, except in the condition that showed the highest resemblance to NREM sleep (rInactive Age IV embryos).

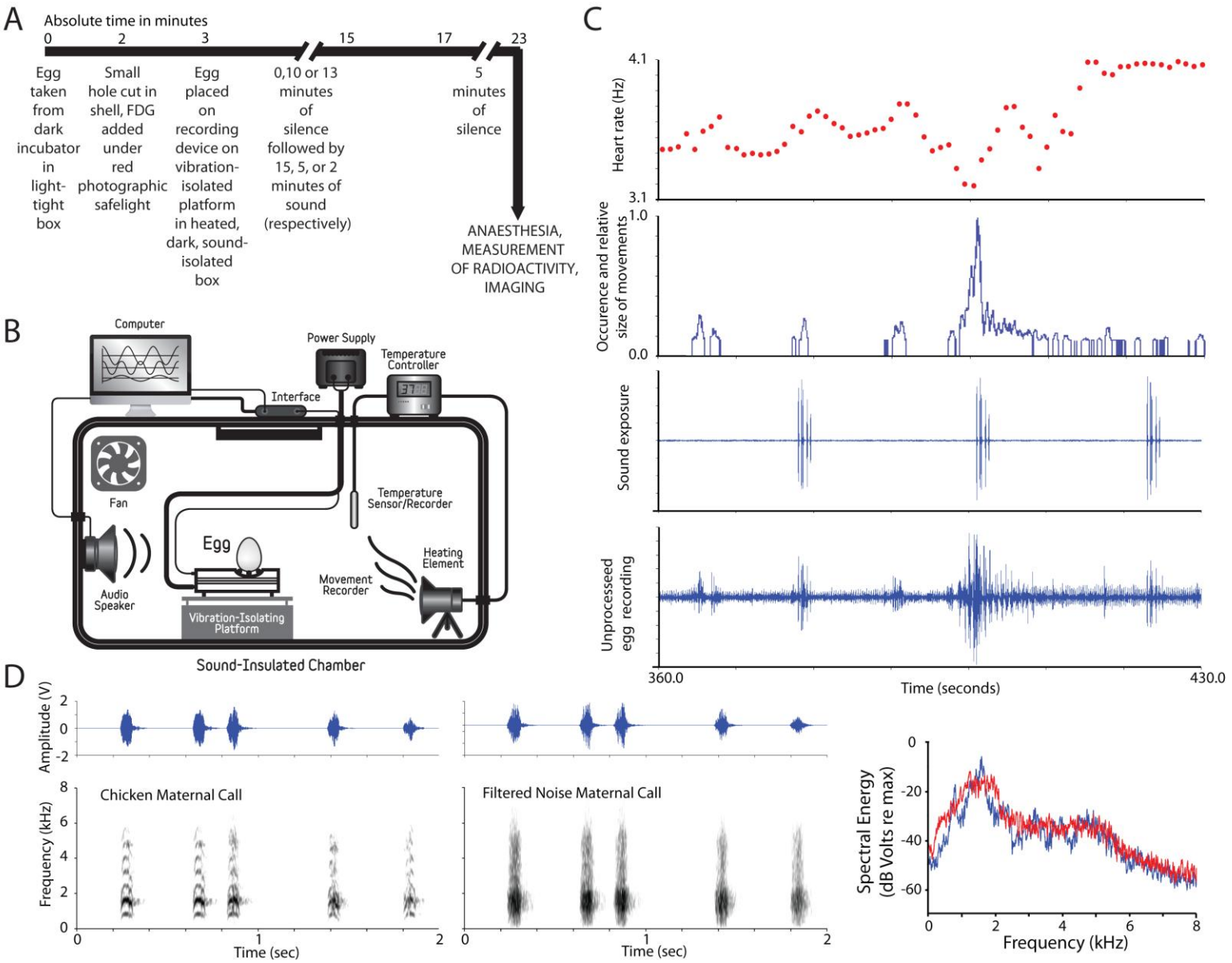
A
Absolute time in minutes
0
2
3
15
17
23
Egg taken from dark incubator in light-tight box
Small hole cut in shell, FDG added under red photographic safelight
Egg placed on recording device on vibration-isolated platform in heated, dark, sound-isolated box
0,10 or 13 minutes of silence followed by 15, 5, or 2 minutes of sound (respectively)
5 minutes of silence
ANAESTHESIA, MEASUREMENT OF RADIOACTIVITY, IMAGING
B
Computer
Power Supply
Temperature Controller
Interface
Fan
Temperature Sensor/Recorder
Egg
Heating Element
Movement Recorder
Audio Speaker
Vibration-Isolating Platform
Sound-Insulated Chamber
C
Heart rate (Hz)
4.1
3.1
Occurence and relative size of movements
1.0
0.0
Sound exposure
Unprocesseed egg recording
360.0
430.0
Time (seconds)
D
Amplitude (V)
Chicken Maternal Call
Filtered Noise Maternal Call
Frequency (kHz)
Time (sec)
Spectral Energy (dB Volts re max)
Frequency (kHz)

Figure S1.

Figure S1. Experimental Details and Sample Data

(A) The time line for the imaging experiments.

(B) Diagram of the experimental setup.

(C) Example of behavioral data recorded from eggs. (Bottom) Raw amplitude [y-axis, arbitrary units] – time (seconds) waveform from a sound-exposed embryo (stimulus amplitude-time waveform, 2nd from bottom), together with the movement-time waveform derived by signal-processing from the raw recording (2nd from top, y-axis units : Volts), and the heart-rate contour also derived by signal processing (top, y-axis units: Hertz).

(D) Sound stimuli used in the experiments (left and middle, amplitude-time (top) and wide-band spectrographic representations (bottom); right, spectral energy [y-axis] versus frequency [x-axis] plot; the chicken stimulus is in blue, the filtered noise stimulus is in red.

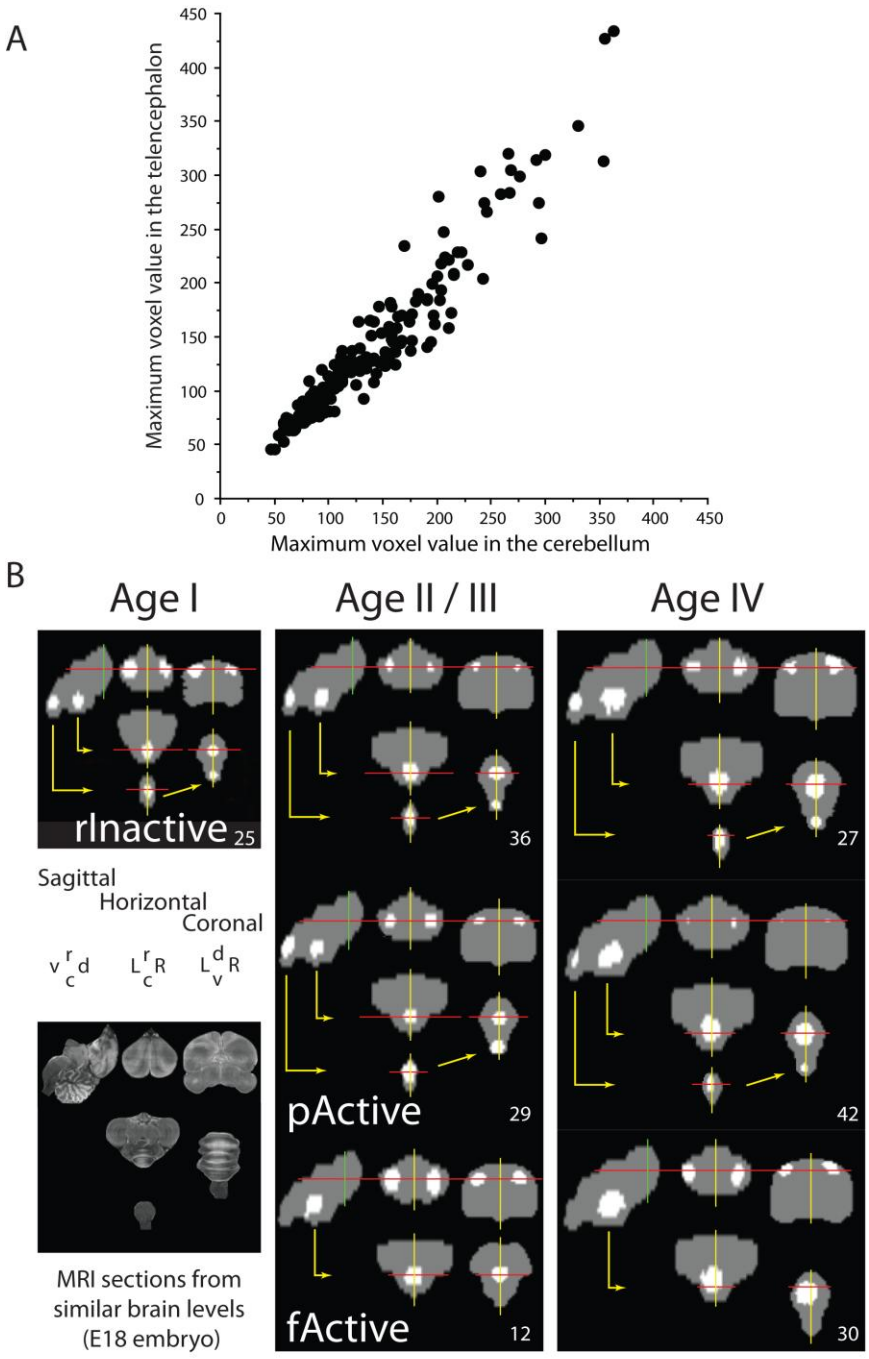

Figure S2. Additional Analyses of Embryo Brain Activation Patterns

(A) Maximum voxel values in the telencephalon (y-axis) and cerebellum (x-axis) for all 201 embryos.

(B) The locations of metabolic activity within 15% of the higher-brain maximum, shared by at least 50% of the embryos within each brain pattern / developmental stage category. Each gray area represents a 2-dimensional projection of the brain from a sagittal, horizontal, or coronal perspective (r = rostral, c = caudal, L = left, R = right, d = dorsal, v = ventral); structural MRI images from similar levels of the brain are shown at the lower left. Numbers are sample sizes.

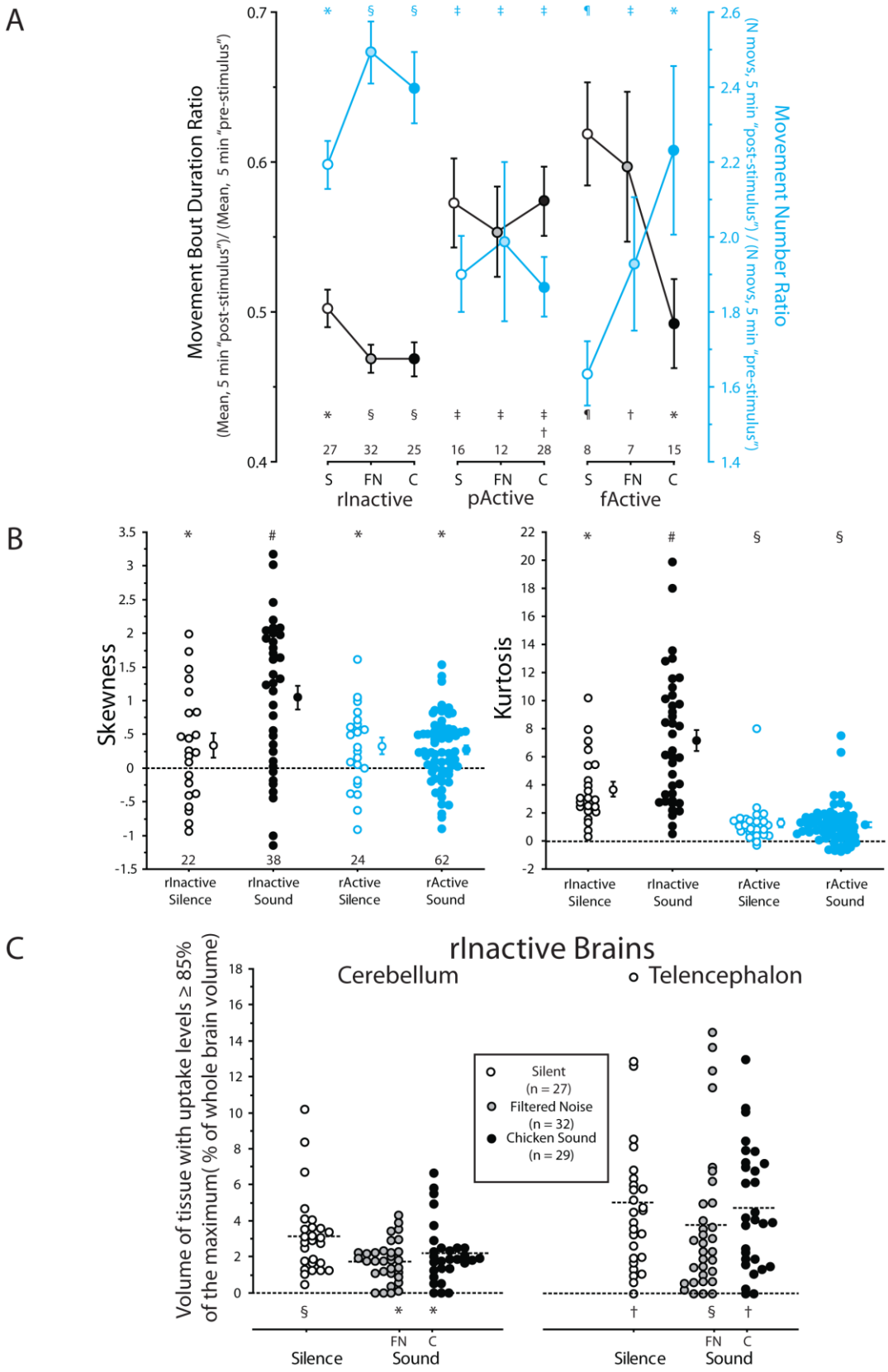
A
Movement Bout Duration Ratio
(Mean, 5 min "post-stimulus")/ (Mean, 5 min "pre-stimulus")
Movement Number Ratio
(N movs, 5 min "post-stimulus") / (N movs, 5 min "pre-stimulus")
0.7
0.6
0.5
0.4
2.6
2.4
2.2
2.0
1.8
1.6
1.4
27 32 25
16 12 28
8 7 15
S FN C
rInactive
pActive
fActive
B
Skewness
Kurtosis
3.5
3
2.5
2
1.5
1
.5
0
-.5
-1
-1.5
22
20
18
16
14
12
10
8
6
4
2
0
-2
22 38 24 62
rInactive Silence
rInactive Sound
rActive Silence
rActive Sound
C
rInactive Brains
Cerebellum
Telencephalon
Volume of tissue with uptake levels ≥ 85% of the maximum(% of whole brain volume)
18
16
14
12
10
8
6
4
2
0
Silent (n = 27)
Filtered Noise (n = 32)
Chicken Sound (n = 29)
Silence
FN
C
Sound

Figure S3.

Figure S3. Additional Analyses of Sound Stimulation Effects on Brain and Behaviour

(A) Movement bout duration ratios (black) and movement number ratios (blue) [y-axis], plotted by brain pattern and stimulus condition [x-axis]. Movement bout duration ratios = mean movement bout duration during the 5 minutes after the stimulus began (or the equivalent time in silence-exposed embryos), divided by the mean movement bout duration 5 minutes before the stimulus began; movement number ratios = the number of movement bouts during the 5 minutes after the stimulus began (or the equivalent time in silence-exposed embryos), divided by the number of movement bouts before the stimulus began. Symbols at the top and bottom of the graph represent the results of post-hoc tests corrected for multiple comparisons based on a Kruskal-Wallis ANOVA (Movement bout duration ratio: $df = 8$, $H = 35.99$, $p < 0.0001$; movement number ratio $H = 45.22$, $df = 8$, $p < 0.0001$); points with different symbols are significantly different from each other ($p < 0.05$ level). Sample sizes are given below each point. Error bars are $\pm$ 1 sem.

(B) Skewness (third moment, left) and kurtosis (fourth moment, right) of the whole-brain distribution of glucose uptake values [y-axis] by brain pattern and stimulus condition [Sound or Silence, x-axis]. The filtered noise and chicken conditions were combined because they exhibited similar distributions. The dots with error bars ($\pm$ 1 sem) are means of the scatterplots to the left of them. Symbols at the top of the graph represent the results of post-hoc tests corrected for multiple comparisons ($p < 0.05$). Sample sizes are given at the bottom of the graph.

(C) Volume (% of whole brain volume) of brain tissue with glucose uptake levels $\geq$ 85% of the maximum value above the rPRF [y-axis] versus sound exposure condition [x-axis] for the cerebellum (left) and telencephalon (right). Dotted lines indicate the mean values of each group. Symbols at the bottom of the graph represent the results of post-hoc tests corrected for multiple comparisons ($p < 0.05$).

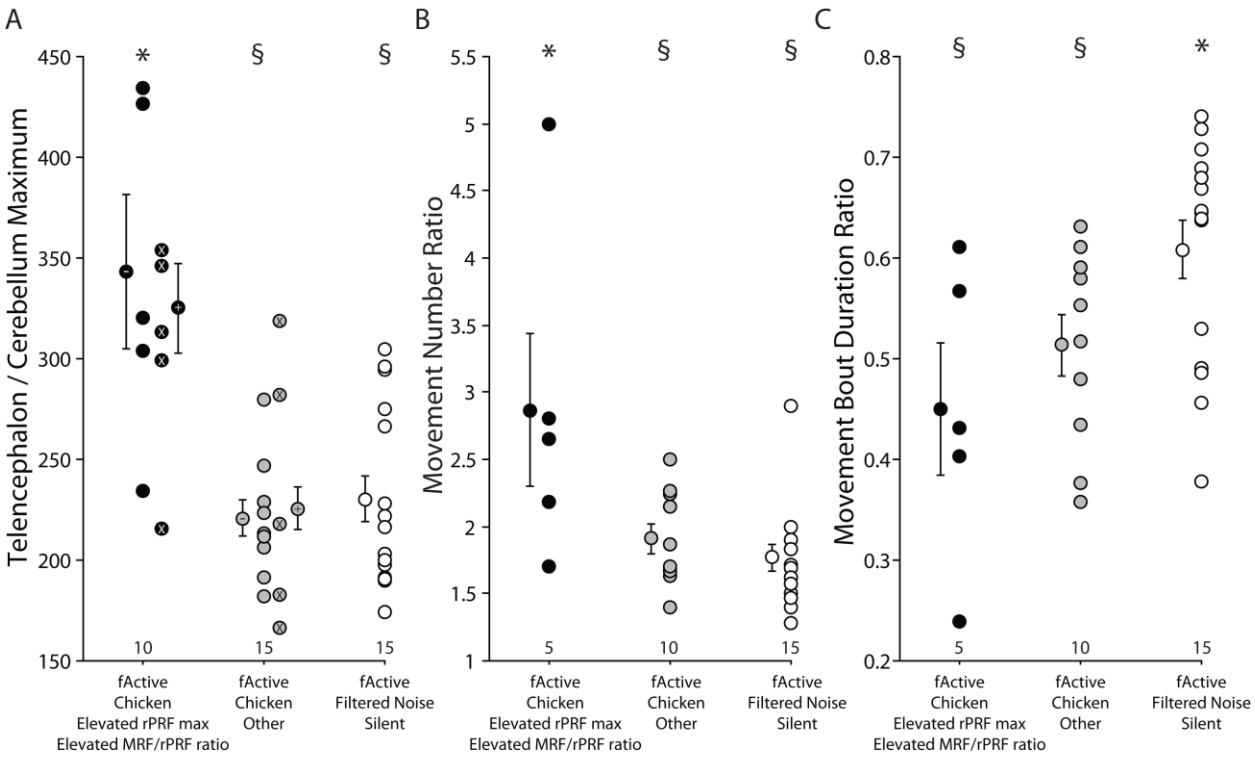

Figure S4. **Additional Analyses of the Effects of Sound Stimulation on fActive Embryo Brain Activation and Behaviour**

(A) The maximum glucose uptake value in the telencephalon or cerebellum (whichever was higher) [y-axis] plotted against three categories of fActive embryos: (leftmost) chicken-stimulated with elevated rPRF and MRF/rPRF ratio values (see Figure 6A), (center) all other fActive chicken stimulated embryos, (rightmost) fActive embryos exposed to filtered-noise or silence. An "x" indicates a data point from an embryo given 15-minute chicken stimulation. Points with error bars ($\pm$ 1 sem) indicate means; "+" includes 15-min birds, "-" excludes them. Symbols at the top of the graph represent the results of post-hoc tests corrected for multiple comparisons ($p < 0.05$; significance indications are the same for tests including or excluding embryos stimulated for 15-min). Sample sizes are given at the bottom of the graph.

(B and C) Movement number ratio (B) and movement bout duration ratio (C) (see Figure S3A) for the same groups shown in (A); error bars, significance designations, and sample sizes are given as above.

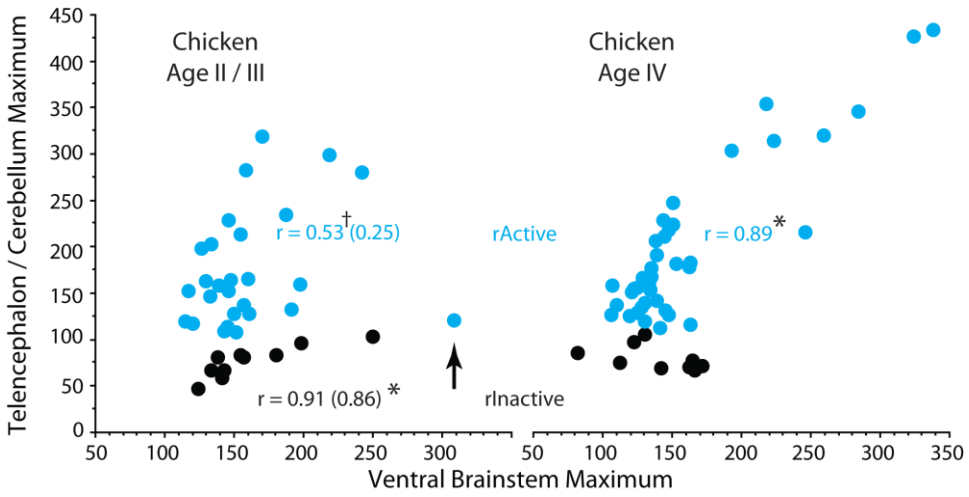

Figure S5. Additional Analyses of the Activity Correlation between Brain Regions

The correlation between maximum values in the telencephalon / cerebellum (whichever had the higher value,[y-axis]) and the ventral brainstem [x-axis]. Data from chicken-stimulated embryos is divided according to developmental stage and brain pattern. The arrow indicates an outlying embryo that was classified as rActive based on its maximal glucose level above the ventral brainstem (Figure 1B), but, based on the other data at its developmental stage, it appears to better fit with the "constrained" glucose uptake levels of rInactive embryos. The correlation values in parentheses are based on counting it as rActive; correlation values outside of parentheses are based on counting it as rInactive. All p-values were corrected for 12 implicit multiple comparisons [2 developmental stages (Ages II/III, and IV) x 2 brain patterns (rInactve, rActive) x 3 stimulus conditions (silence, filtered noise, chicken)]. Only significant values (*) or marginally significant values (†, p = 0.052) are shown.

Supplemental Experimental Procedures

The Choice of Imaging Modality

The primary purpose of this study was to collect information on brain metabolic activity in embryos using the least invasive conditions possible. PET/CT imaging was chosen because it allowed subjects to continue their normal behavior without any constraints while tracer molecules were being taken up by their brain, muscle and organ systems, and because it avoided sensory stimulation confounds due to the noise and vibration associated with functional or structural magnetic resonance imaging. The requirement for minimally- invasive conditions limited us to studying the temporally-integrated uptake of tracer over the entire 20-minute experimental period. This is why behavioral analyses were conducted with reference to relative durations or proportions of events over the whole experimental period. The results obtained here will serve as a reference point for future studies incorporating more invasive manipulations.

Subjects, Their Preparation for Imaging, and Sound Stimuli

All animal use in these experiments was reviewed and approved by the local animal use committee. Data from 223 birds were used for this study. Sixteen of these were 1-2 day-old posthatching birds obtained from a commercial hatchery; the other 207 were obtained as fertilized eggs from commercial sources and incubated as described below. Nine of these 207 embryos were imaged multiple times; the other 198 were imaged only once. The major dataset consisted of 201 embryos, 198 imaged once at various ages, together with the final imaging sessions of 3 multiply-imaged embryos. A diagram of the experimental time-course is shown in Figure S1A.

Of the 201 embryos analyzed here, 51 were imaged after no exposure to sound stimulation (silent condition), 51 after exposure to the filtered-noise stimulus (filtered noise condition, 37 for two minutes, 14 for 5 minutes), and 91 after exposure to the chicken stimulus (chicken condition, 44 for 2 minutes, 24 for 5 minutes, 27 for fifteen minutes). The stimuli used in these experiments are shown in Figure S1D. The chicken stimulus and its post-hatching behavioral validation have been described previously (34, 35). The filtered-noise stimulus was created using the SIGNAL digital sound-analysis system (Engineering Design, Berkeley, CA). The chicken stimulus was converted to the frequency domain, its discrete Fourier transform spectrum was smoothed with a 1 Hz window to create a spectral envelope, this was multiplied by the spectrum of uniform random (white) noise, inverse-transformed to convert it back to the time domain, and adjusted to have the same root-mean-squared (rms) amplitude as the chicken stimulus.

Egg Preparation for Imaging

Fertilized chicken eggs were incubated for 15-21 days (Hamburger-Hamilton stages 39-45 (32)) in a light-tight incubator (Brinsea Octagon 100, Somerset, UK) at 37.5° C, 55 % humidity and removed singly in a light-tight, padded container for behavioral recording and imaging.

A noninvasive method for introduction of tracer molecules was used in order to preserve the integrity of both the fibrous protective inner shell membrane, and the heavily-vascularized chorioallantoic membrane across which gas exchange takes place. 2-deoxy-2-

^{18}Fluoro-D-glucose was obtained in sterile saline solution from commercial sources, and approximately 1.5 mCi was mixed with a sufficient volume of dimethyl sulfoxide (DMSO, Sigma-Aldrich) to make the final solution 10% DMSO by volume. This was placed in a 1.0 cc syringe in a 37.5° C water bath several minutes prior to use. Under a red photographic safelight, a small (4-5 mm diameter) hole was gently cut in the shell overlying the airspace at the blunt end of the egg, and the tracer solution was applied through the hole by depositing it gently on top of the inner shell membrane in the region underlying the hole. A piece of sterile, porous wound-closure tape (3M Steri-strip Elastic Skin Closure, St. Paul, MN, USA) was used to seal up the hole, and the egg was placed on a custom-made movement-recording device (see below) atop a vibration-isolation platform (Minus-K BM-10, Inglewood, CA) inside a light-tight 37.5° C sound-isolated chamber for the 20-minute recording period prior to imaging.

DMSO has been routinely used as a low-toxicity cryoprotective solvent for biological materials, as well as a vehicle for transdermal delivery of human medicines, and has also been reported to suppress glutamate-induced neurotoxicity (56) and oxidative neuronal damage (57) in adult brains. More recently, it was found to be cytotoxic to cultured auditory hair cells prepared from postnatal day 2-3 rat pups after 24 hours of continuous exposure (58), and to affect the neurite outgrowth (but not the survival) of cultured cerebellar cells from 7-day old rat pups (59). A recent study found that intraperitoneal injections of DMSO into young postnatal C57Bl/6 mice at concentrations as low as 0.3 ml/kg increased the proportion of apoptotic cells subsequently found in their brains (60), first detectable at 2 hours after administration. Since DMSO does not appear to affect the survival of cultured neurons, it is unclear if this result reflects a developmentally-vulnerable period for increased brain cell death, or a decrease in the function of microglial cells and macrophages that scavenge dying cells, resulting in the persistence of cells with apoptotic morphology for longer periods of time. We used doses equivalent to ~0.4-0.8 ml/kg, topically applied on a fibrous “external” membrane, rather than injected directly into the body cavity. The 20 minute period between application and imaging, together with the fact that all embryos received equivalent DMSO exposure, indicates that differences in apoptosis are unlikely to explain the differences in brain glucose responses analyzed here. For multiply-imaged embryos (9 total, of which only 3 were used in the main data set), brain glucose uptake responses did not appear to be different than in singly-imaged embryos (Figure 1C).

At the end of the recording period, singly-imaged birds were removed from the sound-isolation chamber under a red photographic safelight, and immediately placed in a light-tight container containing an overdose of volatile isoflurane anesthetic (Baxter Healthcare, Deerfield, IL) for 2 minutes. The egg was then quickly opened, and the embryo head was removed at or below the 6th cervical vertebra with a surgical scissors, and rinsed several times with warm saline. It was next placed in a 25-ml plastic centrifuge tube for measurement of radioactivity (PTW Curimentor Model T-12004-0097, Freiburg, Germany), and finally removed from the tube, and affixed to a cardboard platform for imaging.

For multiply-imaged birds, the egg was removed from the sound-isolation chamber under a red photographic safelight, and placed in a small plastic bag (resistant to isoflurane) that was connected by a tube to a volatile anesthesia dispenser at one end, and vented by a tube connected to an absorption filter canister at the other end. Isoflurane mixed with oxygen (initially 1.5 – 2.0%, adjusted down to 0.5-1.0 % after the first 2-3 minutes) was piped through

the bag, and the bag was inserted into the bore of the PET/CT imager. Imaging was conducted at room temperature (28-30° C) in the dark. The purpose of the lower temperature and anesthesia was to abolish the spontaneous movements given by embryos so that clean PET / CT images could be obtained. At the end of imaging, eggs were quickly removed from the imager and the bag under a red photographic safelight, and were placed back on the movement-recording device in the light-tight 37.5° C sound-isolated chamber for approximately 5 minutes to make sure that their heart rates and spontaneous movement recovered to pre-imaging levels. They were then replaced in the light-tight transport container and taken back to their incubator. On the last imaging session, 3 of these embryos were treated exactly like the singly-imaged birds described above.

Although volatile isoflurane anesthesia has been routinely used in animal work, it has been reported to increase apoptosis in the brains of 7-day-old rat pups exposed to it continuously for 6 hrs (61), visible by 2 hrs after the cessation of anesthesia. This can be counteracted by adding xenon to the volatile gas mixture used for anesthesia (62-64). Isoflurane-induced apoptosis is unlikely to have affected glucose uptake in the present studies, because anesthesia was briefly administered after glucose uptake had already taken place.

Potential Effects of Ionizing Radiation from This Experimental Design

Estimation of radiation dosimetry in small laboratory animals is not straightforward. The activity concentration in animal tissues is high since the injected dose does not scale linearly with weight (65), and the small size of the subject allows a larger fraction of the radiation to escape without interacting with body tissues. Since major organogenesis in chicken embryos occurs prior to day 10 of incubation (66), and the earliest radiation exposure we have performed started on day 16 of incubation, teratogenicity is not expected to occur. In terms of absorbed and equivalent doses, we can approximately equate the size and composition of late-stage chicken embryos to a 20 g mouse. In a chicken embryo CT session, the dose deposited in each subject is less than 40 mSv (31). The worst-case scenario would be for animals that underwent multiple CT scans for developmental staging twice a day for five days, so that the total maximum accumulated dose in those animals would be 400 mSv, still well below dose levels that could become worrisome (67,68) or lethal (the LD50/30 = 7 Gy for small rodents (68,69)). A PET tracer injection in a mouse can produce a whole body dose between 6 and 90 cGy (70). In our experiments the dose was not injected into the subject, but rather deposited on top of the inner shell membrane, and this would result in a much lower dose going into the embryo. Therefore, the cumulative exposure to radiation from both the CT and PET procedures as a result of multiple imaging over the last 4-5 days of incubation is compatible with normal development, and the exposure for a single PET/CT imaging session is negligible.

Posthatching Bird Preparation for Imaging

The posthatching birds were used in a preliminary study to examine the feasibility of PET imaging in young chicks. One-to-two-day-old posthatching birds were obtained on their day of hatching and kept in a group in a heated container with free access to food and water prior to imaging. Immediately prior to being introduced singly into a dimly-lit sound-isolation chamber at 32° C, they were injected intramuscularly with 100-280 μCi of 2-deoxy-2-^{18}Fluoro-D-glucose in sterile saline into the body of their breast (pectoralis) muscle. Once in the chamber, they

were exposed to 20 minutes of either the chicken sound (Figure S1B), presented in the same way as in the embryo experiments, or a similar sound constructed from Japanese quail (*Coturnix coturnix japonica*) vocalizations, used in previous experiments (34, 35). After a 20-minute sound exposure period, they were left in silence for a further 10 minutes, then given a lethal overdose of Equithesin anesthesia intramuscularly injected into the pectoralis muscle prior to PET imaging. No CT images were taken of these posthatching animals. Video recordings of the behavior of all individuals revealed that none of them visibly slept during the recording period; they all spent roughly equivalent amounts of time emitting "contact call" vocalizations, and exploring the interior of the chamber.

Behavioral/Cardiac Activity Recording and Analysis

The noninvasive movement-recording device for embryo behavior was based on an earlier design (33) in which three monoaural piezoelectric phonograph cartridges (Fox-Indelson Model 2145-ZST, Madrid) were arranged in a triangle with their styli pointing upwards to hold the egg under study. The egg was positioned (blunt end up) on top of the three styli, which held it in place. The stylus cartridges were connected in parallel; the common signal arising from the three transducers was first amplified with a gain of 60, and then passed through three filtering stages to eliminate electrical interference due to AC power and noise. The first stage was a bandpass filter from 0.05 Hz to 1 KHz used to attenuate both low- and high-frequency noise. The second and the third filtering stages were notch filters, eliminating AC contamination at 50 Hz, and its first harmonic at 100 Hz. The signal was amplified by a factor of 10 between the two notch filters. The output was connected to one channel of a two-channel USB audio digitizer interface (Edirol UA-1A, Los Angeles, CA); a copy of the output to the speaker in the sound-isolation chamber (Figure S1B) was connected to the other channel, so that embryo movement recordings and a record of the stimulation delivered to the embryo were captured simultaneously. Signals were digitized at 44.1 kHz, and were displayed in real time on the computer screen and saved using Audacity v.1.2.6 software (Carnegie Mellon University, Pittsburgh, PA).

Movement recordings were processed using custom-written programs in the SIGNAL digital sound-analysis system. Each recording had any DC offset removed, and a copy was prepared for movement analysis by downsampling (point decimation) by a factor of 10, lowpass filtering at 600 Hz, and resampling to a 2000 Hz sampling rate using cubic spline interpolation. The resulting file is referred to below as the "prepared movement file". A spectrogram of this file was made from 0-30 Hz (discrete Fourier transform (DFT) length 8192 points). Heartbeat activity on these spectrograms consisted of a stack of harmonically-related components at frequencies that were integer multiples of the heart rate; the spectral contour detection algorithm in SIGNAL was used to extract the frequency-time contour of the heartbeat harmonic component with the greatest power. This contour was divided by the harmonic number of the component it was extracted from to yield the fundamental frequency-time contour of the heartbeat, and resampled using cubic spline interpolation to a sampling rate of 2000 Hz. The heart rate – time contour was used to analyze both heart rate changes and the coefficient of variation of the heartbeat.

Another copy of the prepared movement file was processed in two stages to derive an amplitude envelope-time contour for the heartbeat. First, the prepared movement file was

absolute-valued, and visually examined to select a threshold value for the highest-amplitude heartbeat deflection in the recording. An automated program then identified all of the time intervals exceeding this value, and reset them to the value of the highest-amplitude heartbeat value. This altered file was then visually examined to see if there were any remaining portions of the file with lower heartbeat amplitude values that had movement deflections evident, and these portions of the file were reiteratively treated as above until a relatively smooth waveform was obtained for the entire 20 minute recording period. In the second stage, this waveform was smoothed with a 4 sec window and then visually examined after being replotted on top of the original prepared movement file, to make sure that it accurately reflected the amplitude envelope of the heartbeat over the entire recording. Once this fit was satisfactory, an automated program added 10% of the maximum value of this smoothed heart amplitude envelope contour to all of its time points; the result served as a threshold-time contour that had to be exceeded in order for a voltage deflection to be counted as a movement.

A final movement-time contour file was derived by an automated program that took a new copy of the prepared movement file, absolute-valued it, identified time periods that did not exceed their respective values in the threshold-time contour, and set these to zero. Another automated program compiled data on movement bouts and quiescent periods from these final movement-time contours; a quiescent period was defined as an interval between two movements that was $\geq$ 150 msec in duration, and a movement bout consisted of any set of movements separated by less than 150 msec from each other. This program produced a file containing a sequential list of each movement bout and quiescent period duration, and the integrated voltage sum and average voltage/msec (measures of movement size) for each movement bout. An example of an unprocessed egg recording, together with sound stimulation, movement and heartbeat information processed from it are shown in Figure S1C.

Movement and quiescent period bout duration statistics (Figure 4A,B) were calculated by an automated program written in MATLAB (The Mathworks, Natick, MA), which constructed histograms of duration values for each individual recording (quiescent period bins starting from $100*2^n$... msec, where n= 0,1...13, and movement bout bins starting from 0, $100*2^n$... msec, where n = 1,2...13), then calculated the best-fitting exponential and power-law curves for each histogram, and saved the fit statistics and r^2 values into a list file. A fit was declared when one function had significantly ($p < 0.05$) or, in one case, marginally-significantly ($p < 0.06$) better mean fits than the other function AND explained an average of > 90% of the variance. Whenever these conditions were not met, the fit was declared to be indeterminate.

PET/CT Imaging and Image Analysis

Embryos were scanned with the ARGUS PET/CT scanner (30, 31). Samples were located at the center of the field of view (FOV) of the PET system and scanned for 60 minutes with a 400-700 keV energy window. Images were obtained using a 3D-OSEM algorithm with a spatial resolution of 0.7 mm (71). Once the PET scan was over, the bed supporting the sample was automatically moved by a mechanical linear slide to the center of the X-ray computed tomograph (CT) FOV, and was immediately scanned with the tube set at 250 μA and kilovoltages between 35 and 45 keV, depending on the characteristics of the sample. The scanning took nine minutes, and the data were reconstructed using an optimized FDK cone reconstruction (72). The whole process was performed using an integrated console (MMWKS, (54)) that allowed the visualization and

manipulation of the datasets in 3 dimensions, provided analysis tools (segmentation, quantification) as well as visualization tools (registration, multimodality fusion and volumetric rendering), and also provided export and import methods for dataset handling. The console generated intrinsically-registered PET/CT images when both scans were done serially, and also provided co-registration tools based on fiducial marks for manual registration, and based on mutual information (MI) methods for automatic processing (55).

Posthatching animals were scanned with the ATLAS small animal PET scanner (73), and the images were reconstructed by ramp-filtered backprojection from 2D sinograms, with a 3D-OSEM algorithm that achieved an in-plane resolution better than 1.8 mm (74).

CT Image Analysis

CT images were processed for fine-scale developmental staging of the embryos by first removing all extraneous material other than the head from the image (the supporting stage of the imager, the cardboard platform the heads were attached to, any debris) using both user-assisted and automated programs written in ImageJ (U.S. National Institutes of Health, Bethesda, MD). Since the studies were conducted over an extended period of time, there was a possibility that small amounts of drift in CT scanner calibration values could interact with nonlinear developmental changes in the degree of bone calcification to produce unwanted classification errors. For this reason, the thresholding procedure for isolating the skeleton used a proportional criterion based on two reference points, instead of choosing an absolute Hounsfield Unit (HU) value. The HU value for completely mineralized bone in low kilovoltage CT images is at least 10 times larger than muscle tissue, which would be too high to segment the still-calcifying bones of the chicken skull. Setting the threshold to an intermediate level that depended on the actual value of brain/skin/muscle ensured that cartilage was not included, but that more mineralized bone was, and that the level of calcification demanded for inclusion was as uniform as possible across embryos of all ages.

The value for thresholding the skeleton was determined automatically by a program written in ImageJ that made a histogram of the HU values treated as gray levels (256 intensity bins) in the isolated head CT image, and found two points in this histogram: the most common gray level (G_s, which represents the average gray level of brain/skin/muscle tissue), and the maximum value starting from 10 intensity bins above this (G_c, the start of the range where cartilaginous structures began to stand out above brain/skin/muscle tissue). Empirical comparison of the results of different threshold values with the timetable of known calcification events in chick embryo skull development (75-77), and of the head morphology with the standard embryological stages of Hamilton and Hamburger (32), led to the selection of a value = 0.25*(Gs+Gc) for inclusion into the skeleton, which was uniformly applied to all embryos. All points in the CT image above this threshold were set to a value of 1, with all other points set to 0. The resulting image was then filtered (hybrid 3D median filter) and despeckled to remove noise using ImageJ; it is referred to as the “skeletal mask”.

User-assisted programs written in ImageJ and MMWKS were used to make isolated images of two groups of bony structures from the skeletal mask: (a)”vertebral”- the atlas, axis and first three cervical vertebrae, and (b) “basal skull”- the rostroparasphenoid, alaparasphenoid, basiparasphenoid, basioccipital, sphenoid, and exoccipital bones. An automated program written in IDL (ITT Visual Information Solutions, White Plains, NY) was used

to calculate the total volume in mm^3 of each of these bony structure groups. Once all 201 skeletons were processed in this fashion, the basal skull (y-axis) and vertebral (x-axis) values were plotted against each other, and the first principal component was taken. This accounted for 98.5% of the variance in the basal skull-vertebral volume plot; the projection values of each embryo skeleton on the first principal component were used as a measure of developmental stage (Skeletal Age Value, Figure 2A).

PET Image Analysis

Reconstructed PET images were first validated for measurement purposes. The total sum of intensity values in the head on the image was compared to the radioactivity measured in the head immediately prior to imaging by fitting a line to these data with a y-intercept at 0. This was done separately for images collected on different machines, and for images collected on the same machine using different software calibration regimes, yielding a total of four groups of images. The linear fit explained 99.3 % of the variance in one of these cases, and 99.5% of the variance in the three others, demonstrating that the intensity values on the images quantitatively represented the concentration of radioactive glucose in the head of the embryo.

In order to have a common scale of measurement for glucose uptake in brain tissue that would be independent of the total amount of glucose that was made available to the brain, image values were normalized by referencing them to the maximum uptake value found in the pituitary gland, a structure that was clearly visible on all PET images. Maximum values were used because these could be measured automatically in a consistent way, without having to develop criteria for outlining the entire structure to assure equivalent sampling in different embryos. The chick pituitary is connected to the brain, receives a similar blood supply, and is highly metabolically active throughout this period of development (78). A linear regression on log-log coordinates revealed that the maximum pituitary value explained 99.6% of the variance in brain maximum voxel values, with a slope of 1.0. The normalized but spatially untransformed images are referred to below as “normalized reconstructions”.

Brain maxima values were extracted directly from the normalized reconstructions using the segmentation tools in the MMWKS Analysis module. While viewing the 3-D PET image, a threshold was continuously adjusted so as to reveal the cluster of voxels with the highest maximum intensity in the brain / spinal cord rostral to the first cervical vertebra. If this cluster was at or caudal to the rostral pontine reticular formation (rPRF), the threshold was readjusted until a cluster appeared somewhere else in the brain. In order to be counted as a maximum, a volume element (voxel) had to occur as part of a cluster of at least 3 voxels that could be thresholded out from the brain tissue that immediately surrounded them. The position of all such clusters within the nervous system was confirmed by examining their position in a combined CT-PET 3-D image using the “Fused Display” in the MMWKS Registration module.

For other measurements, brains were divided by the developmental stages defined in the text (Ages I, II/III and IV, Figure 2A). Ages II and II were combined to improve statistical power, based on the high similarity of their maximum brain activation patterns (Figure S2B), and because Age III appears to represent the culmination of trends starting in Age II that peak in the population during a brief period just prior to the transition to air-breathing. Age IV was further subdivided into an “early” and “late” stage (with 55 and 54 embryos, respectively). An embryo whose developmental stage was in the center of each of these 5 groups was chosen as

a “standard spatial template” for the group, and the cleaned CT images of the heads of these 5 embryos were put into a standard position and orientation using the “Reformatting Tool” in MMWKS. A custom-written program in IDL that called the library of reformatting tool commands in MMWKS was then used to sequentially align and scale the cleaned head CT image of each embryo to the template CT image for its group in two steps, first using the rigid MI alignment routines of MMWKS, and then using the rigid-plus-scaling alignment, and storing a file containing the spatial transformation values. All alignments were checked visually using the “Fused Display” in the MMWKS Registration module and modified if necessary. Alignment transformations were also calculated among sequential pairs of the standard spatial templates for these groups.

Once these alignments had been obtained for all embryos, the spatial transformation values were used to align all of the normalized PET images, which are referred to below as “spatially-aligned PET images”. For the 16 posthatching birds, the bird with the brain of median size was chosen, and its brain was aligned to the spatially-aligned PET image of the “late stage” Age IV standard using the same procedure as above; the other 15 posthatching birds were then aligned to it. A template for the whole brain was created for each group by making a mean PET image from the spatially-aligned PET images of all birds in the group (to average out individual variation), and this mean image was then thresholded at the lowest value for which all brain structures were included in the masks for all developmental groups (= 105 normalized units). The skull CT image of the standard template was then used to mask out any areas that were not within the skull. These “whole-brain” templates were used for the measurements illustrated in Figure S1D (the basis for assigning glucose activation pattern designations), and for measuring the distribution of brain glucose uptake values shown in Figures 2B, and Figures S2B and S3B,C. These measurements were captured using custom-written programs in IDL.

Measurements of the regions of interest (ROIs) shown in Figure 2B used the spatially-aligned PET images. The ROIs were created using the mean spatially-aligned PET image from Age II/III; the rPRF ROI was created by thresholding this image at a value of 125 normalized units and masking all activations outside the rPRF; the MRF ROI was created by subtracting the mean spatially-aligned PET images of the rInactive embryos from those of the pActive embryos and masking all activations that were below zero or clearly outside the mesencephalic reticular formation. These ROIs were then spatially transformed to the other groups so that a common set of ROIs was used for all measurements.

For measuring volumes of activation within 15% of the brain maximum (Figures S2B and S3C), the normalized reconstructions were used to produce spatial masks of these regions by thresholding at 0.85 of the maximum value above the rPRF, and removing any areas that were outside of the skull. These masks were then spatially transformed to their developmental stage standards using the spatial transformation values described above.

Eye (iris) muscle and jaw (mandibular depressor) muscle activations (Figure 4C,D) were measured from the normalized reconstructions for each embryo. The eye value was derived by taking the mean value of all voxels with an intensity $\geq$ 50 normalized units bilaterally in the region bounded 3-dimensionally by the iris ring bones, which were visible in the CT images of all embryos. The mandibular depressor muscle was also visible bilaterally in all embryos as two discrete spheres of activation on each PET image; these were demarcated using the “Region

Growing" tool in the MMWKS Analysis module with a threshold of 70 and seeds placed on the center of the activation for each muscle. The bilateral average of the intensity values was used.

Statistical Tests

This study was designed to examine large-scale pattern changes in glucose uptake over all ages and stimulus conditions. Because of the large degree of variation in overall glucose uptake levels and the "patchy" spatial distribution of high-uptake areas in the brains studied here, the PET data set as a whole did not meet the assumptions required for applying statistical parametric mapping techniques (SPM, 79). Instead of applying the extensive spatial smoothing required to make these data suitable for SPM, we applied standard statistical analyses using measurements taken on unsmoothed data.

All statistical comparisons used nonparametric statistical tests corrected for multiple comparisons (all p-values were two-tailed). Frequency comparisons were done using the G-test, corrected for continuity with the Williams correction (80), except in cases where one of the categories had zero frequency, in which case Fisher's exact tests (80) were used. Log-linear analysis (80) was used to analyze 3-way frequency data (Figure 5C). These frequency analyses were conducted using BIOMstat (Exeter Software, Setauket, NY). Nonparametric 2-way analysis of variance (used to analyze the Age II/III data in Figure 4D) was conducted according to the Scheirer-Ray-Hare extension of the Kruskal-Wallis test (80). Kruskal-Wallis one-way analysis of variance with post-hoc tests corrected for multiple comparison (75) were carried out in Statview 5 (SAS, Cary, NC) and Matlab, as were correlations, partial correlations, Mann-Whitney tests (81), and Wilcoxon matched-pair sign-rank tests (81). For all correlations, both Pearson product-moment (r) and Spearman rank correlations (ρ) were calculated, and both the magnitude and significance of these tests agreed with each other; the Pearson values are reported here.

Supplemental References

56. Jacob, S.W., and de la Torre, J.C. (2009) Pharmacology of dimethyl sulfoxide in cardiac and CNS damage. Pharmacol. Rep. 61, 225-235.

57. DiGiorgio, A.M., Hou, Y., Zhao, X., Zhang, B., Lyeth, B.G., and Russell, M.J. (2008) Dimethyl sulfoxide provides neuroprotection in a traumatic brain injury model. Restor. Neurol. Neuros. 26, 501-507.

58. Qi, W., Ding, D., and Salvi, R.J. (2008). Cytotoxic effects of dimethyl sulfoxide (DMSO) on cochlear organotypic cultures. Hearing Res. 236, 52-60.

59. Götte, M., Hofmann, G., Michou-Gallani, A.I., Glickman, J.F., Wishart, W., and Gabriel, D. (2010) An imaging assay to analyze primary neurons for cellular neurotoxicity. J. Neurosci. Meth. 192, 7-16.

60. Hanslick, J.L., Lau, K., Noguchi, K.K., Olney, J.W., Zorumski, C.F., Mennerick, S., and Farber, N.B. (2009) Dimethyl sulfoxide (DMSO) produces widespread apoptosis in the developing central nervous system. Neurobiol. Dis. 34, 1-10.

61. Jevtovic-Todorovic, V., Hartman, R.E., Izumi, Y., Benshoff, N.D., Dikranian, K., Zorumski, C.F., Olney, J.W., and Wozniak, D.F. (2003) Early exposure to common anesthetic agents causes widespread neurodegeneration in the developing rat brain and persistent learning deficits. J. Neurosci. 23, 876-882.

62. Ma, D., Williamson, P., Januszewski, A., Nogaro, M.C., Hossain, M., Ong, L.P., Shu, Y., Franks, N.P., and Maze, M. (2007). Xenon mitigates isoflurane-induced neuronal apoptosis in the developing rodent brain. Anesthesiology 106, 746-753.

63. Cattano, D., Williamson, P., Fukui, K., Avidan, M., Evers, A.S., Olney, J.W., and Young, C. (2008) Potential of xenon to induce or to protect against neuroapoptosis in the developing mouse brain. Can. J. Anesth. 55, 429-436.

64. Shu, Y., Patel, S.M., Pac-Soo, C., Fidalgo, A.R., Wan, Y., Maze, M., and Ma, D. (2010) Xenon pretreatment attenuates anesthetic–induced apoptosis in the developing brain in comparison with nitrous oxide and hypoxia. Anesthesiology 113, 360-368.

65. Jagoda, E.M., Vaquero, J.J., Seidel, J., Green, M.V., and Eckelman, W.C. (2004) Experiment assessment of mass effects in the rat: implications for small animal PET imaging. Nucl. Med. Biol. 31, 771-779.

66. Romanoff, A.L. (1960) The Avian Embryo: Structural and Functional Development (New York: Macmillan).

67. Malladi, S.M., Bhilwade, H.N., Khan, M.Z., and Chaubey, R.C. (2007) Gamma ray induced genetic changes in different organs of chick embryo using peripheral blood micronucleus test and comet assay. Mutat. Res. 630, 20–27.

68. Ford, N.L., Thornton, M.M., and Holdsword, D.W. (2003) Fundamental image quality limits for microcomputed tomography in small animals. Med. Phys. 30, 2869–2877.

69. Obenaus, A., and Smith, A. (2004) Radiation dose in rodent tissues during micro-CT imaging. J. X-Ray Sci. Technol. 12, 241–249.

70. Hildebrandt, I.J., Su, . I. J., and Weber, W.A. (2008) Anesthesia and other considerations for in vivo imaging of small animals. ILAR J. 49, 17-26.

71. Herráiz, J.L., España, S., Vaquero, J.J., Desco, M., and Udías, J.M. (2006) FIRST: Fast iterative reconstruction software for (PET) tomography. Phys. Med. Biol. 51, 4547-4565.

72. Abella, M., Vaquero, J.J., Sisniega, A., Pascau, J., Udías, J.M., García, V., Vidal, I., and Desco, M. (2011) Software architecture for multi-bed FDK-based reconstruction in x-ray CT scanners. Comput. Meth. Prog. Bio., in press, 1-15, http://dx.doi.org/10.1016/j.bbr.2011.03.031.

73. Seidel, J., Vaquero, J.J., and Green, M.V. (2003) Resolution uniformity and sensitivity of the NIH ATLAS small animal PET scanner: Comparison to simulated LSO scanners without depth-of-interaction capability. IEEE T. Nucl. Sci. 50, 1347-1350.

74. Johnson, C.A., Seidel, J., Carson, R.E., Gandler, W.R., Sofer, A., Green, M.V., and Daube-Witherspoon, M.E.(1997) Evaluation of 3D reconstruction algorithms for a small animal PET camera. IEEE T. Nucl. Sci. 44, 1303-1308.

75. Parker, W.M. (1869) On the structure and development of the skull of the common fowl (Gallus domesticus). Philos. T. Roy. Soc. 159, 755-807.

76. Jollie, M.T. (1957) The head skeleton of the chicken and remarks on the anatomy of this region in other birds. J. Morphol. 100, 389-436.

77. Hogg, D.A. (1990) The development of pneumatisation in the skull of the domestic fowl (Gallus gallus domesticus). J. Anat. 169, 139-151.

78. Parkinson, N., Collins, M.M., Dufresne, L., and Ryna, A.K. (2010) Expression patterns of hormones, signaling molecules, and transcription factors during adenohypothesis development in the chick embryo. Dev. Dynam. 239, 1197-1210.

79. Friston, K.J., Ashburner, J.T., Kiebel, S.J., Nichols, T.E., and Penny, W.D. (2007) Statistical Parametric Mapping: The Analysis of Brain Functional Images, (New York: Academic Press).

80. Sokal, R.R., and Rohlf, F.J. (1995) Biometry: The principles and practice of statistics in biological research, 3rd Edition, (New York: Freeman).

81. Siegel, S., and Castellan, N.J. Jr. (1988) Nonparametric Statistics for the Behavioral Sciences, 2nd Edition, (New York: McGraw-Hill).